# A High-Speed Sliding-Mode Observer for the Sensorless Speed Control of a PMSM

Hongryel Kim, Jubum Son, and Jangmyung Lee, *Senior Member, IEEE*

***Abstract*—This paper proposes a sensorless speed control strategy for a permanent-magnet synchronous motor (PMSM) based on a new sliding-mode observer (SMO), which substitutes a sigmoid function for the signum function with a variable boundary layer. In order to apply a sensorless PMSM control which is robust against parameter fluctuations and disturbances, a high-speed SMO is proposed, which estimates the rotor position and the angular velocity from the back EMF. In the conventional SMO, a low-pass filter and an additional position compensation of the rotor are used to reduce the chattering problem that is commonly found in the SMO using the signum function. In order to overcome the time delay caused by the low-pass filter, in this research, a sigmoid function is used for the switching function instead of the signum function. Also, the variation in the stator resistance is estimated to improve the steady-state performance of the SMO. The stability of the proposed SMO was verified using the Lyapunov second method to determine the observer gain. The validity of the proposed high-speed PMSM sensorless velocity control has been demonstrated with simulations and real experiments.**

***Index Terms*—Estimation, Lyapunov function, permanent-magnet synchronous motor (PMSM), sensorless control, sigmoid function, sliding-mode observer (SMO).**

## I. Introduction

RECENTLY, for highly efficient industrial machines, robots, and automobiles, the usage of alternating-current (ac) motors instead of direct-current (dc) motors has been increasing rapidly. An ac motor has a more complex control system than that of a dc motor. However, since there is no brush in an ac motor, the size of the ac motor can be smaller with the same power and the lifetime is much longer than that of a dc motor. There are two types of ac motors: the induction motor (IM) and the permanent-magnet (PM) synchronous motor (PMSM). The PMSM is very popular in ac motor applications since it is useful for various speed controls. The IM has a simple structure, and it is easy to build. However, it is not as efficient as the PMSM considered in terms of dynamic performance and power density [1].

Since a PMSM receives a sinusoidal magnetic flux from the PM of the rotor, precise position data are necessary for an efficient vector control. Generally, the rotor position can be detected by a resolver or by an absolute encoder. However, these sensors are expensive and very sensitive to environmental constraints such as vibration and temperature [2]. To overcome these problems, instead of using position sensors, a sensorless control method has been developed for control of the motor using the estimated values of the position and velocity of the rotor [3]–[12].

In a conventional sliding-mode observer (SMO), a low-pass filter and an additional position compensation of the rotor are used to reduce the chattering problem commonly found in SMOs using a signum function. Currently, a sigmoid function is used for the SMO as a switching function. The observer has fast responses and has a robustness inherent in the design parameters [13], [14]. In this observer, the chattering, which happens at the observer using the signum function, has been reduced significantly [15]. The stator resistance needs to be estimated by the Lypunov function intermediate equations so as to prove the stability of the observer. The stator resistance changes during motor operation, which deteriorates the control performance, unless it is compensated for in real time [8]. The cascade control method has been proposed for the achievement of an accurate tracking performance [16], and high-gain observers have been designed to estimate the states under a scalar disturbance [17]. A hybrid terminal SMO design method is proposed to achieve sensorless drive for a PMSM [18], and a tuning method is proposed in order to obtain high-speed and high-accuracy positioning systems [19]. The general schemes of sliding-mode control have been well surveyed recently [20]. Most of the observer designs focus on the fast response and high tracking accuracy. For the fast response, the use of a sigmoid function in a boundary layer is popular. However, the observer error cannot be guaranteed to converge to zero within the boundary layer [18], [21], [22], [24].

This paper proposes a new sensorless control algorithm for a PMSM based on the new SMO which uses a sigmoid function as a switching function with variable boundary layers. Using this SMO, the position and velocity of the rotor can be calculated from the estimated back EMF [25]. Also, to overcome the sensitivity of the parameter variations in the sensorless control and to improve the steady-state performance, the stator resistance is estimated using an adaptive control scheme. The superiority of the proposed algorithm has been proved by comparison with the conventional SMO through real experiments.

This paper consists of five sections, including the introduction.

Section II introduces the conventional SMO, and Section III proposes the new SMO. Section IV illustrates the experimental

Manuscript received January 23, 2010; revised August 20, 2010; accepted November 21, 2010. Date of publication December 10, 2010; date of current version August 12, 2011.

H. Kim and J. Lee are with Pusan National University, Busan 609-735, Korea (e-mail: kimhr2580@pusan.ac.kr; jmlee@pusan.ac.kr).

J. Son is with LS Industrial System, Anyang 431-749, Korea (e-mail: sonjb81@pusan.ac.kr).

Color versions of one or more of the figures in this paper are available online at http://ieeexplore.ieee.org.

Digital Object Identifier 10.1109/TIE.2010.2098357

results, and Section V draws the conclusions relating to the contributions of this paper and also makes proposals for future research work.

## II. Conventional SMO

### A. PMSM Modeling

In the case of PMSM sensorless control, the fixed-frame model of the stator needs to be developed, regardless of the rotor position.

The PMSM consists of a rotor with a PM and a stator with a three-phase Y-connected winding, which is located at every 120° on the circle. The three-phase motor is an intrinsically nonlinear time-varying system. However, it can be simplified to a two-phase model, assuming that the imaginary part is negligible in the Y-connected windings [13]. For PMSM sensorless control, the rotor position is estimated so the stator equations can be used to model the system.

The state equations, where the stator current is a state variable of the fixed-frame voltage equation, can be represented as

$$\begin{aligned}\dot{i}_\alpha &= -\frac{R_s}{L_s}i_\alpha - \frac{1}{L_s}e_\alpha + \frac{1}{L_s}v_\alpha \\ \dot{i}_\beta &= -\frac{R_s}{L_s}i_\beta - \frac{1}{L_s}e_\beta + \frac{1}{L_s}v_\beta\end{aligned} \tag{1}$$

where $i_{\alpha,\beta}$, $e_{\alpha,\beta}$, and $v_{\alpha,\beta}$ represent the current, electromotive force, and voltage for each phase, respectively, in the fixed frame. $R_s$ and $L_s$ represent the stator resistance and inductance, respectively.

The electromotive force for each phase can be represented in the fixed frame as

$$\begin{aligned}e_\alpha &= -\lambda_f \omega_r \sin\theta \\ e_\beta &= \lambda_f \omega_r \cos\theta\end{aligned} \tag{2}$$

where $\lambda_f$, $\omega_r$, and $\theta$ represent the magnetic flux of the PM, the electric angular velocity, and the rotor angle, respectively.

### B. Conventional SMO

The sliding-mode control is used to restrict the state variables on the sliding surface by changing the system structure dynamically. It is widely used for nonlinear system control since it is robust against system parameter variations. For the sensorless control of the PMSM, the sliding-mode controller is adopted for use in the observer design and so is named the SMO. However, there are the shortcomings of chattering and time delay for the rotor position compensation in the conventional SMO [7], [8], [18].

Fig. 1 shows the conventional sliding-mode controller where the signum function is used as the switching function and the low-pass filter (LPF) is used to eliminate the chattering effects from the switching. The conventional SMO uses the Lyapunov function; it is the control method used to estimate the position and speed of the rotor at the same time.

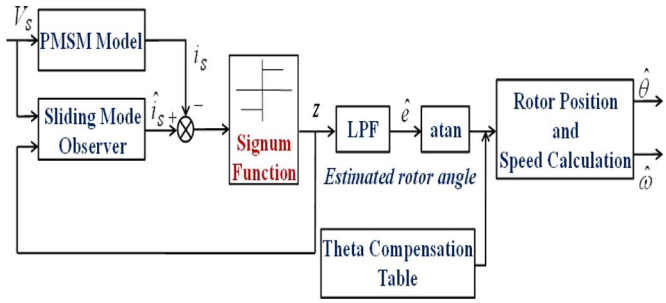


Fig. 1. Conventional SMO.

## III. High-Speed SMO

The SMO using the signum function as the switching function suffers from chattering. Therefore, before the back EMF is estimated, the output of the SMO needs to be passed through the LPF, which causes a time delay and requires extra compensation for the rotor position estimation. The chattering causes some fluctuations in the steady-state response. This happens particularly when the variations of the estimated parameters are large at the high-speed region; the observer gain needs to be increased to reduce large ripples on the estimated parameters. This may result in uncontrollable situations [15]. To eliminate the undesirable chattering, a sigmoid function is adopted in this research as the switching function, requiring neither the LPF nor the extra compensator for the rotor position. In order to compensate for the time delay caused by the fact that the arithmetical speed of the sigmoid function is slower than that of the signum function, a variable observer gain is used. This new SMO provides robustness against the uncertainties of the system parameters by pushing the system states on the sliding surface.

### A. Sigmoid Function

This new SMO is composed by the PMSM current equation in the rest frame of (1) as follows:

$$\begin{aligned}\dot{\hat{i}}_\alpha &= -\frac{\hat{R}_s}{L_s}\hat{i}_\alpha + \frac{1}{L_s}v_\alpha - \frac{1}{L_s}kH(\hat{i}_\alpha - i_\alpha) \\ \dot{\hat{i}}_\beta &= -\frac{\hat{R}_s}{L_s}\hat{i}_\beta + \frac{1}{L_s}v_\beta - \frac{1}{L_s}kH(\hat{i}_\beta - i_\beta).\end{aligned} \tag{3}$$

The new SMO resolves the problems of the conventional SMO by using a sigmoid function as the switching function. The sigmoid function is represented as

$$\begin{bmatrix} H(\bar{i}_\alpha) \\ H(\bar{i}_\beta) \end{bmatrix} = \begin{bmatrix} \left(\frac{2}{1+\exp(-a\bar{i}_\alpha)}\right) - 1 \\ \left(\frac{2}{1+\exp(-a\bar{i}_\beta)}\right) - 1 \end{bmatrix} \tag{4}$$

where $a$ is a positive constant used to regulate the slope of the sigmoid function. The estimation errors of the stator current are defined as $\bar{i}_\alpha = \hat{i}_\alpha - i_\alpha$ and $\bar{i}_\beta = \hat{i}_\beta - i_\beta$.

### *B. Stability Analysis*

The sliding surface $s_n$ can be defined as functions of the errors between the actual current, i.e., $i_\alpha$ and $i_\beta$, and the estimated current, i.e., $\hat{i}_\alpha$ and $\hat{i}_\beta$, for each phase as follows:

$$S_n = [s_\alpha \quad s_\beta]^{\mathrm{T}} = [\hat{i}_\alpha - i_\alpha \quad \hat{i}_\beta - i_\beta]^{\mathrm{T}} \tag{5}$$

where $s_\alpha = \bar{i}_\alpha$ and $s_\beta = \bar{i}_\beta$.

When the sliding mode is reached, i.e., when the estimation errors are on the sliding surface, the estimation errors become zero, i.e., $\hat{i}_\alpha = i_\alpha$ and $\hat{i}_\beta = i_\beta$. At that moment, the sliding surface becomes $S_n = 0$ and the observer becomes robust against the system parameters and disturbances.

Let us find the conditions for the sliding mode. For the PMSM sensorless control, the Lyapunov function used to find the sliding condition can be defined as

$$V = \frac{1}{2} S_n^{\mathrm{T}} S_n + \frac{1}{2}(\hat{R}_s - R_s)^2 \tag{6}$$

where $(1/2)(\hat{R}_s - R_s)^2$ is used to estimate the stator resistance which is a variable parameter. From the Lyapunov stability theorem [8], the sliding-mode condition can be derived to satisfy the condition that $\dot{V} < 0$ for $V > 0$. Taking the time derivative of (6), we find

$$\dot{V} = S_n^{\mathrm{T}} \dot{S}_n + (\hat{R}_s - R_s)\dot{\hat{R}}_s. \tag{7}$$

By using the current equations of (3) in the stationary coordinates, the derivatives of the estimated phase currents can be represented as

$$\begin{aligned}
\dot{\bar{s}}_\alpha &= \dot{\bar{i}}_a = \dot{\hat{\bar{i}}}_\alpha - \dot{\bar{i}}_\alpha \\
&= (\hat{A} - A)\hat{\bar{i}}_\alpha + A(\hat{\bar{i}}_\alpha - \bar{i}_\alpha) + \frac{1}{L_s} e_\alpha - \frac{1}{L_s} kH(\bar{i}_\alpha) \\
\dot{\bar{s}}_\beta &= \dot{\bar{i}}_\beta = \dot{\hat{\bar{i}}}_\beta - \dot{\bar{i}}_\beta \\
&= (\hat{A} - A)\hat{\bar{i}}_\beta + A(\hat{\bar{i}}_\beta - \bar{i}_\beta) + \frac{1}{L_s} e_\beta - \frac{1}{L_s} kH(\bar{i}_\beta)
\end{aligned} \tag{8}$$

where $\hat{A} = -\hat{R}_s/L_s$ and $A = -R_s/L_s$.

By substituting (8) into (7), the sliding condition can be represented as

$$\begin{aligned}
\dot{V} = [\bar{i}_\alpha \quad \bar{i}_\beta] \begin{bmatrix} (\hat{A}-A)\hat{\bar{i}}_\alpha + A(\hat{\bar{i}}_\alpha - \bar{i}_\alpha) + \frac{1}{L_s}\left[e_\alpha - kH(\bar{i}_\alpha)\right] \\ (\hat{A}-A)\hat{\bar{i}}_\beta + A(\hat{\bar{i}}_\beta - \bar{i}_\beta) + \frac{1}{L_s}\left[e_\beta - kH(\bar{i}_\beta)\right] \end{bmatrix} \\
+ \overline{R}_s \cdot \dot{\hat{R}}_s < 0
\end{aligned} \tag{9}$$

where $s_\alpha = \bar{i}_\alpha$, $s_\beta = \bar{i}_\beta$, and $\overline{R}_s = \hat{R}_s - R_s$.

To satisfy the condition $\dot{V} < 0$, (9) is decomposed into two equations as follows:

$$[\bar{i}_\alpha \quad \bar{i}_\beta] \begin{bmatrix} (\hat{A} - A)\hat{\bar{i}}_\alpha \\ (\hat{A} - A)\hat{\bar{i}}_\beta \end{bmatrix} + \overline{R}_s \cdot \dot{\hat{R}}_s = 0 \tag{10}$$

$$[\bar{i}_\alpha \quad \bar{i}_\beta] \begin{bmatrix} A(\hat{\bar{i}}_\alpha - \bar{i}_\alpha) + \frac{1}{L_s}\left[e_\alpha - kH(\bar{i}_\alpha)\right] \\ A(\hat{\bar{i}}_\beta - \bar{i}_\beta) + \frac{1}{L_s}\left[e_\beta - kH(\bar{i}_\beta)\right] \end{bmatrix} < 0. \tag{11}$$

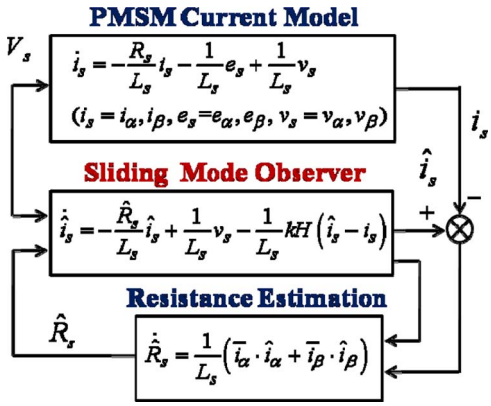


Fig. 2. SMO with the stator-resistance estimation.

From the condition used to satisfy (10), the estimation of the stator resistance can be obtained as

$$\dot{\hat{R}}_s = \frac{1}{L_s}(\bar{i}_\alpha \cdot \hat{i}_\alpha + \bar{i}_\beta \cdot \hat{i}_\beta). \tag{12}$$

It should be noted that this estimation of stator resistance is directly related to the stability of the system.

Fig. 2 shows the SMO with the stator-resistance estimation. The stator resistance is estimated by integrating (12). Using this estimated value of the variable stator resistor in the current control, the steady-state performance can be further improved [14].

In order to keep the SMO stable, the observer gains should satisfy the inequality condition found in (11). This condition in (11) is described in more detail as follows:

$$\begin{aligned}
-\frac{R_s}{L_s}\left((\bar{i}_\alpha)^2 - (\bar{i}_\beta)^2\right) + \frac{1}{L_s}\left(e_\alpha \bar{i}_\alpha - \bar{i}_\alpha kH(\bar{i}_\alpha)\right) \\
+ \frac{1}{L_s}\left(e_\beta \bar{i}_\beta - \bar{i}_\beta kH(\bar{i}_\beta)\right) < 0
\end{aligned} \tag{13}$$

where the observer gain can be derived to satisfy the inequality condition as

$$k \geq \max\left(|\hat{e}_\alpha|, |\hat{e}_\beta|\right). \tag{14}$$

The chattering problem in the sliding-mode control is solved by using the proposed observer that applies the sigmoid function as the switching function and changes the observer gain. The sigmoid functions are in a certain range given by $-1 < H(\bar{i}_\alpha) < 1$ and $-1 < H(\bar{i}_\beta) < 1$ while the signum functions are either $-1$ or 1, which are multiplied by the suitable gain $k$ so as to satisfy the Lyapunov stability condition. When the switching frequency is kept constant at 5 kHz, the number of switches in an electric angle period is reduced for the high speed as compared with the low-speed rotation. Therefore, it is necessary to adjust the observer gain according to the switching delay [23]. Fig. 3 shows how the boundary layer is changed according to the rotational velocity. The width of the boundary layer becomes wider with an increase of the number of revolutions per minute in order to guarantee the response time for the switching. When the width is kept constant regardless of the number of revolutions per minute, a high amount of chattering occurs at a high speed with an increase of the response time;

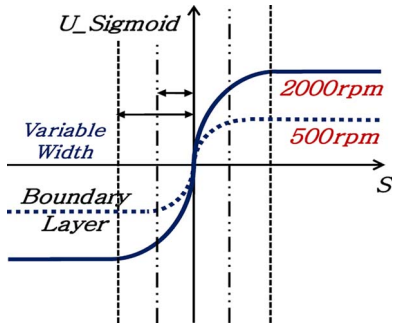


Fig. 3. Variable boundary layers according to the velocity.

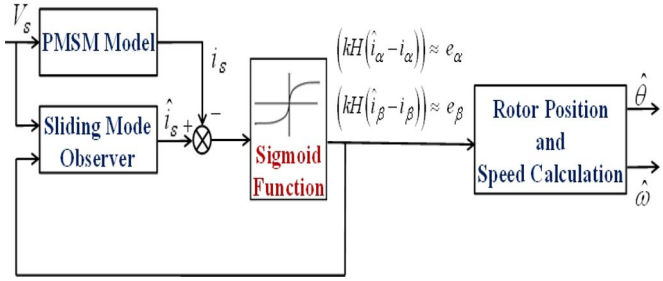


Fig. 4. SMO with the sigmoid function and estimation calculation.

the steady-state error becomes large at a low speed. Therefore, the observer gain $k$ is adjusted according to the rotational velocity as

$$k_{\mathrm{va}} = k \cdot w_{\mathrm{ref}} \tag{15}$$

where $w_{\mathrm{ref}}$ is determined heuristically and $k_{\mathrm{va}}$ replaces the $k$ in (3).

### C. Position and Velocity Estimation of the Rotor

The sliding mode occurs with the suitable selection of observer gain $k$; thus, the sliding surface can be represented as

$$[\dot{s}_\alpha \quad \dot{s}_\beta]^{\mathrm{T}} = [s_\alpha \quad s_\beta]^{\mathrm{T}} \approx [0 \quad 0]. \tag{16}$$

From the aforementioned equation, the back EMF voltages can be expressed in the form

$$\begin{aligned} \left(kH(\bar{i}_\alpha)\right) &\approx e_\alpha \\ \left(kH(\bar{i}_\beta)\right) &\approx e_\beta. \end{aligned} \tag{17}$$

Fig. 4 shows the block diagram of the new SMO. To resolve the chattering problems, the sigmoid function is serially connected to the sliding-mode control.

Using the estimated back EMF voltages, the position and velocity of the rotor are calculated from

$$\hat{\theta} = -\tan^{-1}\left(\frac{\hat{e}_\alpha}{\hat{e}_\beta}\right) \tag{18}$$

$$\hat{\omega} = \frac{d}{dt}\hat{\theta}. \tag{19}$$

The proposed observer reduces the influence of the estimation error caused by the parameter changes in the conventional adaptive control and calculates the position and the speed of the rotor using the new SMO without the integral operations inherent in the LPF. As a result, the system speed performance is improved. It should be noted that the integral operations, which are basically the digital filters in an actual system, are performed [13] in the conventional observer so as to estimate the position and speed of the rotor. It should also be noticed that, since the digital LPF causes a time delay, the performance of the system goes down.

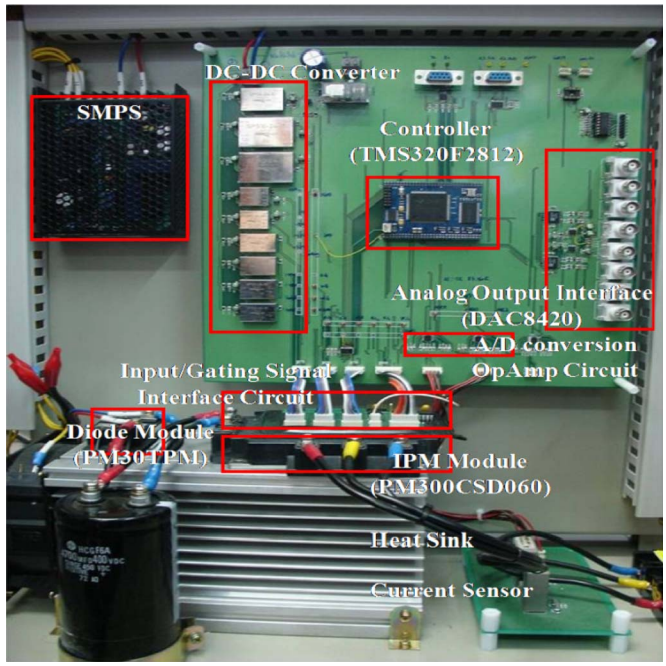


Fig. 5. Sensorless speed controller for the 1-kW PMSM.

## IV. Experimental Results

### A. Hardware Organization

The experimental system was designed to control the CSMT-10 B (1-kW) sinusoidal PMSM (SPMSM) motor made by Samsung Rockwell.

Fig. 5 shows a photograph of the sensorless speed controller for the 1-kW PMSM. PM300CSD060 interior PM (IPM) modules, made by Mitsubishi, are utilized as the switching devices. In order to satisfy the 100-$\mu$s current control cycle, a 1-ms velocity control cycle and a 2-$\mu$s dead time are chosen for the PWM switching and a TMS320F2812 module is used for the main arithmetic unit. To provide the dc power to the IPM, PM30TPM diode modules and 4700-$\mu$F capacitors are used to rectify the ac power. To isolate the upper controller from the gating circuit noise, photocoupler circuits were designed. All of the control variables are monitored by an oscilloscope after they are converted to analog signals through the digital-to-analog (D/A) converter.

The sensorless speed controller implemented by the TMS320F2812 is illustrated in detail, including the SMO.

Fig. 6 shows the block diagram of the sensorless speed controller, where the SMOPOS represents the SMO used to estimate the rotor position. To control the PMSM, the three-phase

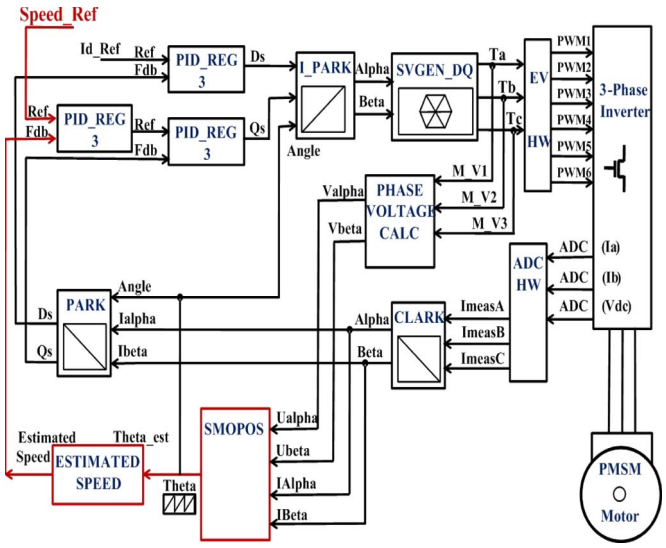


Fig. 6. Block diagram of the sensorless speed controller.

TABLE I
SPECIFICATIONS OF THE PMSM

| Motor constants | | Control Parameter | |
|---|---|---|---|
| Power | 1 [KW] | Poles | 8 |
| Torque | 9.36 [N·m] | Flux | 0.09 [wb] |
| Speed | 3000 [r/min] | Speed Control Period | 1ms |
| Current | 5.4 [A] | Current Control Period | 100 $\mu s$ |
| Input Voltage (DC) | 310 [V] | Current Limit | 20.0 [A] |
| Stator Resistor | 0.25 [Ω] | a | 0.05494 |
| Stator Inductor | 1.3 [mH] | Conventional SMO gain | 25 |
| Rotor Inertia | $1.53 \times 10^{-4}$ [kg·m$^2$] | Proposed SMO gain | 70 |
| Electrical Constant | 5.4 [ms] | Mechanical Constant | 0.27 [ms] |

coordinates need to be transformed into $d$–$q$ synchronous coordinates, which are a part of the vector control. As a result of the vector control, a reference current is generated and passed to the stator of the motor through the inverter, as shown in Fig. 6. In order to make the current to the stator sinusoidal, an space-vector pulsewidth modulation (SVPWM) is adopted. It will be noted that the SVPWM has a high switching speed and an excellent linearity. Using the error between the command and estimated velocities, the proportional–integral–differential (PID) control law is implemented. The PID control is also used for the current control. The SMO, using the sigmoid function as a switching function, estimates the rotor angle from the back EMF. It is also used for the current estimations.

Table I shows the specifications of the CSMT-10 B (1-kW) SPMSM made by Samsung Rockwell. For the switching device operations, PM300CSD060 IPM modules made by Mitsubishi Corporation were used. As the main processor on the control

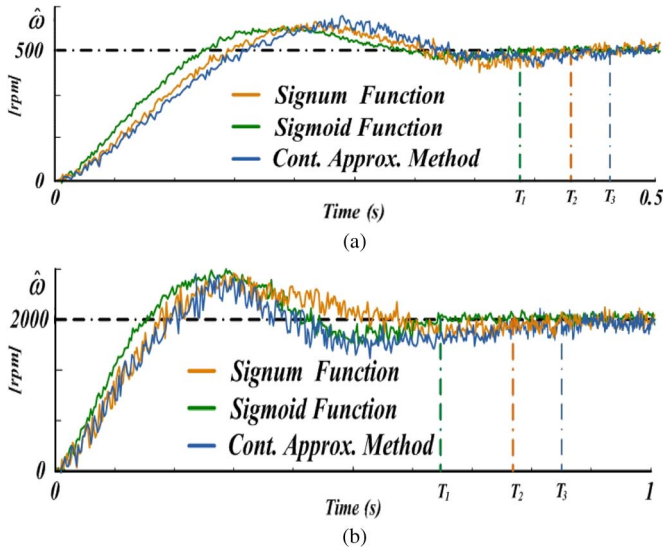


Fig. 7. Responses of the observer using signum and sigmoid functions. (a) Comparison of the step responses for 500 r/min. (b) Comparison of the step responses for 2000 r/min.

board, a TMS320F2812 module of TI Corporation was used, which enables settings of 100 $\mu$s as the current control cycle, 1 ms as the velocity control cycle, and 2 $\mu$s as the dead time. To provide the dc power for the IPM, an inverter circuit was designed using a PM30TPM diode module and a 4700 $\mu$F high-density capacitor. In order to eliminate the noise from the gating signal circuit in the experiments, photocouplers were used to isolate the upper controller from the lower inverter circuit. The control parameters were monitored by an oscilloscope after the D/A conversion.

### *B. Simulation and Experimental Results*

In order to show the high-speed performance of the proposed SMO, it is necessary to compare it with the conventional SMO through the simulations carried out in terms of step responses.

Fig. 7 compares the step responses of two step inputs, 500 and 2000 r/min without a load, between the conventional sliding mode and the proposed SMO. The settling time, which is the time it takes to reach the steady state, with less than a 2% error, is marked on the graph for each algorithm as $T_1$ and $T_2$.

Allowing for the same 20% overshoot with the 500-r/min step size, the proposed SMO has a settling time of 350 ms while the conventional one has one of 400 ms, which is a 50-ms improvement (12.5%), as shown in Fig. 7(a). For the 2000-r/min step size, the proposed observer has a 450-ms settling time while the conventional one has a 550-ms one, which is a 100-ms improvement (about 18%). It can be noted that for high-speed operation, the proposed observer has a greater improvement percentage. This implies that the proposed SMO is well suited for high-speed operations while the conventional observer suffers from a large time delay.

The steady-state performance of the SMO is also important for the steady-state response, since the reduction of the chattering is a critical factor for the SMO. Therefore, the steady-state performances of the two SMOs are again compared at 500 and 2000 r/min.

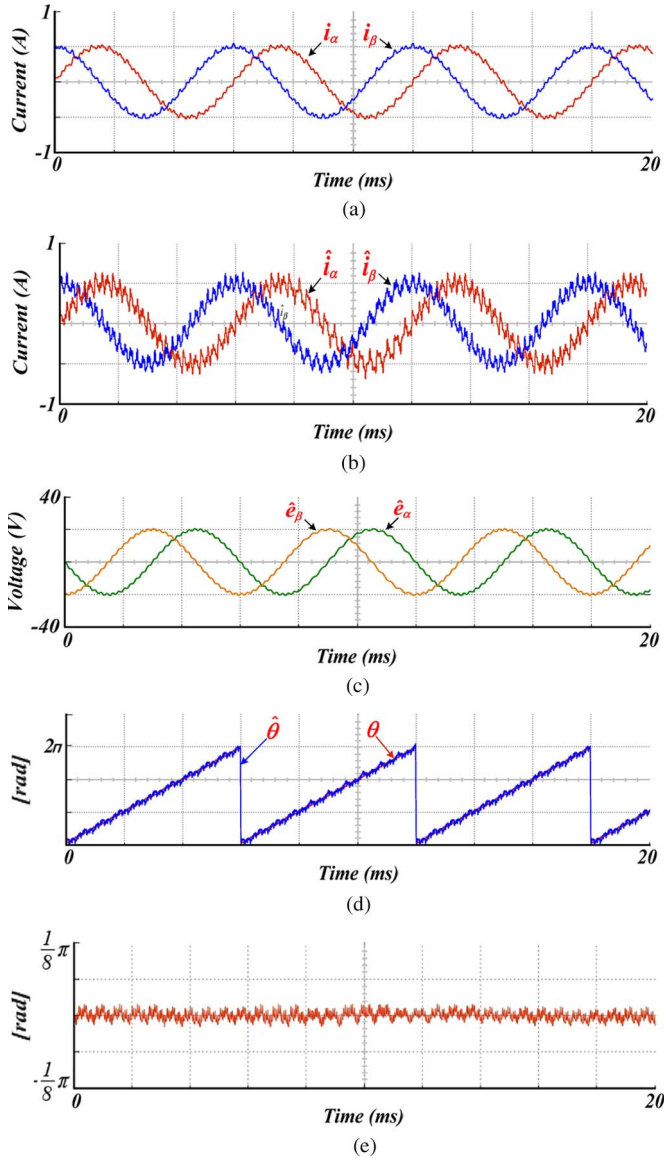


Fig. 8. Sensorless speed control using the signum function at 500 r/min. (a) $i_\alpha$ and $i_\beta$. (b) $\widehat{i}_\alpha$ and $\widehat{i}_\beta$. (c) $\widehat{e}_{\boldsymbol{\alpha}}$ and $\widehat{e}_{\boldsymbol{\beta}}$. (d) $\theta$ and $\hat{\theta}$. (e) Estimation error of $\theta$.

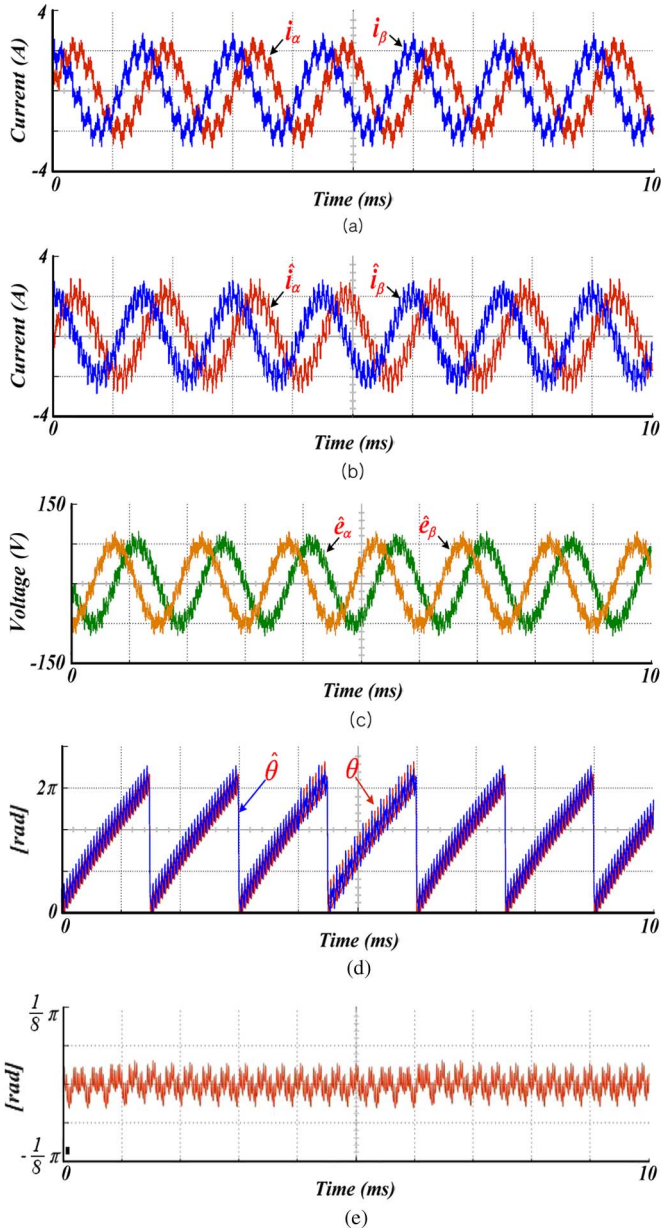


Fig. 9. Sensorless speed control using the signum function at 2000 r/min. (a) $i_\alpha$ and $i_\beta$. (b) $\hat{i}_\alpha$ and $\hat{i}_\beta$. (c) $\widehat{e}_{\boldsymbol{\alpha}}$ and $\widehat{e}_{\boldsymbol{\beta}}$. (d) $\theta$ and $\hat{\theta}$. (e) Estimation error of $\theta$.

Fig. 8 shows the experimental results of the sensorless speed control using the signum function at 500 r/min, Fig. 8(a) shows the real currents, Fig. 8(b) shows the estimated currents, Fig. 8(c) shows the estimated back EMF, Fig. 8(d) shows the actual and estimated rotor position, and Fig. 8(e) shows the estimation error of the rotor position. The 500-r/min motor command velocity corresponds to 33 Hz for the rotor. Therefore, the 100-$\mu$s current control cycle is fast enough to guarantee a steady-state response. The estimated back EMF has a sinusoidal waveform that gives a satisfactory sensorless control.

Fig. 9 shows the experimental results of the sensorless speed control using the signum function at 2000 r/min. Fig. 9(a) shows the real currents, Fig. 9(b) shows the estimated currents, Fig. 9(c) shows the estimated back EMF, Fig. 9(d) shows the actual and estimated rotor position, and Fig. 9(e) shows the estimation error of the rotor position. The 2000-r/min motor command velocity corresponds to 133 Hz for the rotor. Therefore, the 100-$\mu$s current control cycle is not fast enough to guarantee the steady-state response. The estimated back EMF does not have a sinusoidal waveform and so does not give a satisfactory sensorless control.

Fig. 10 shows the experimental results of the proposed sensorless speed control using the sigmoid function at 500 r/min. Fig. 10(a) shows the real currents, Fig. 10(b) shows the estimated currents, Fig. 10(c) shows the estimated back EMF, Fig. 10(d) shows the actual and estimated rotor position, and Fig. 10(e) shows the estimation error of the rotor position. The 500-r/min motor command velocity corresponds to 33 Hz for the rotor. Therefore, the 100-$\mu$s current control cycle is fast enough to guarantee the steady-state response. The estimated back EMF has a sinusoidal waveform that gives a satisfactory sensorless control.

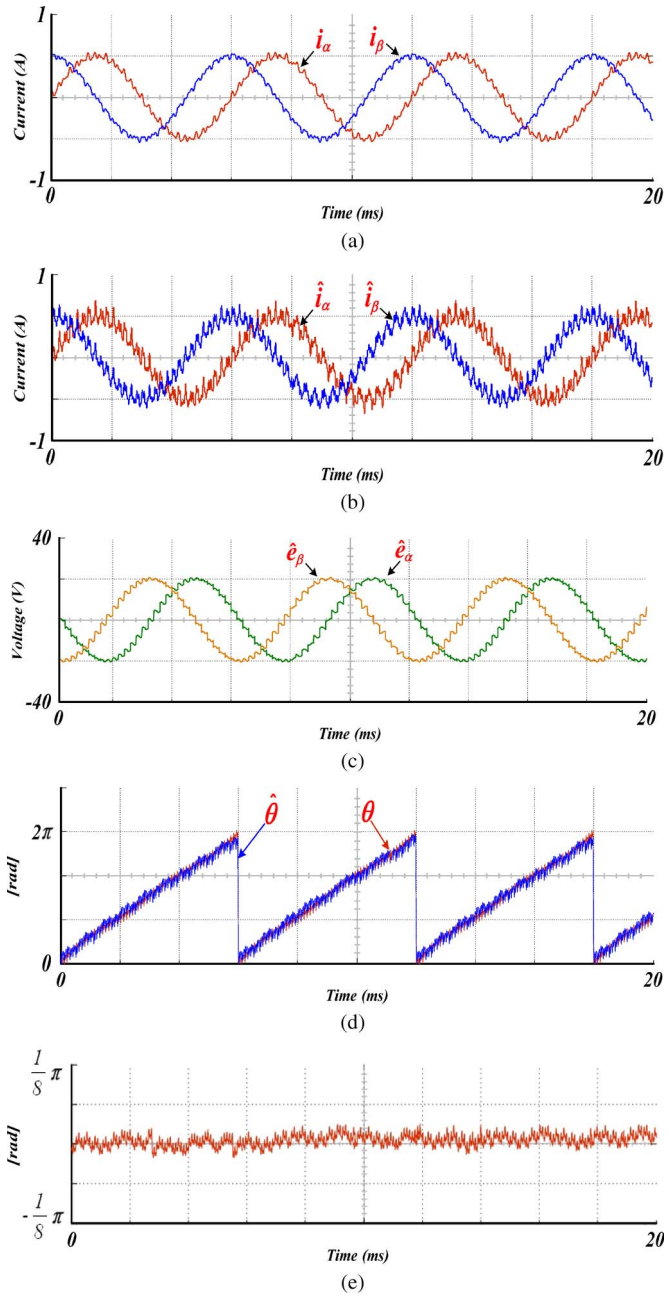


Fig. 10. Proposed sensorless speed control at 500 r/min. (a) $i_\alpha$ and $i_\beta$. (b) $\hat{i}_\alpha$ and $\hat{i}_\beta$. (c) $\widehat{e}_{\boldsymbol{\alpha}}$ and $\widehat{e}_{\boldsymbol{\beta}}$. (d) $\theta$ and $\hat{\theta}$. (e) Estimation error of $\theta$.

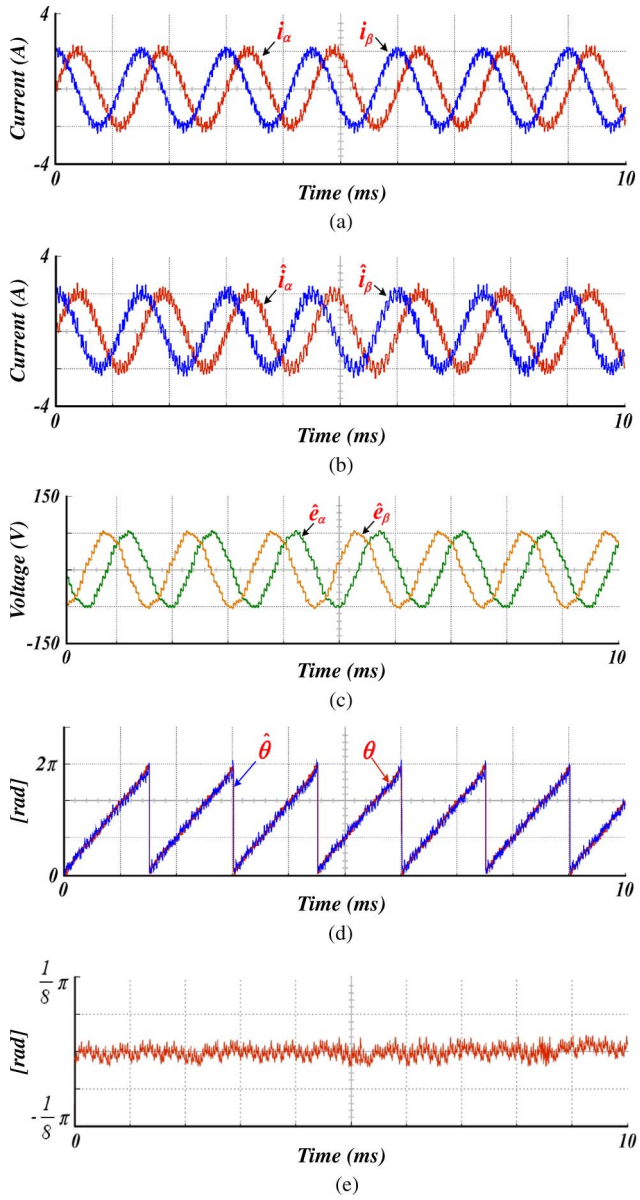


Fig. 11. Proposed sensorless speed control at 2000 r/min. (a) $i_\alpha$ and $i_\beta$. (b) $\hat{i}_\alpha$ and $\hat{i}_\beta$. (c) $\widehat{e}_{\boldsymbol{\alpha}}$ and $\widehat{e}_{\boldsymbol{\beta}}$. (d) $\theta$ and $\hat{\theta}$. (e) Estimation error of $\theta$.

Fig. 11 shows the experimental results of the proposed sensorless speed control using the sigmoid function at 2000 r/min. Fig. 11(a) shows the real currents, Fig. 11(b) shows the estimated currents, Fig. 11(c) shows the estimated back EMF, Fig. 11(d) shows the actual and estimated rotor position, and Fig. 8(e) shows the estimation error of the rotor position. The 2000-r/min motor command velocity corresponds to 133 Hz for the rotor. Comparing Fig. 11 with Fig. 9, it is very clear that there are no large ripples at the estimated currents and the estimated back EMF has a clear sinusoidal waveform, which reduces the steady-state error.

Fig. 12 shows the estimation error characteristics with the signum and sigmoid functions under the loading condition, $J_L = 22.3\ \text{kg} \cdot \text{cm}^2$. Comparing Fig. 12 with Figs. 9(d) and (e) and 11(d) and (e), it is noticed that the loading does not have severe effects on the tracking performance, even though it slows down the step response a little. The estimation error of $\hat{\theta}$ becomes a little larger, which is caused by the slower response.

In order to show the effects of using the estimated stator-resistance value in the current control, the stator resistor is changed artificially from 0.25 to 0.5 Ω.

Fig. 13(a) shows how the proposed SMO estimates the changed resistance. It takes about 0.5 s to estimate the changed resistance precisely, within a 2% error range. Fig. 13(b) shows that a steady-state error happens in the velocity control without a proper estimation of the stator resistance, while Fig. 13(c) shows that the proposed controller recovers the desired velocity within 0.5 s.

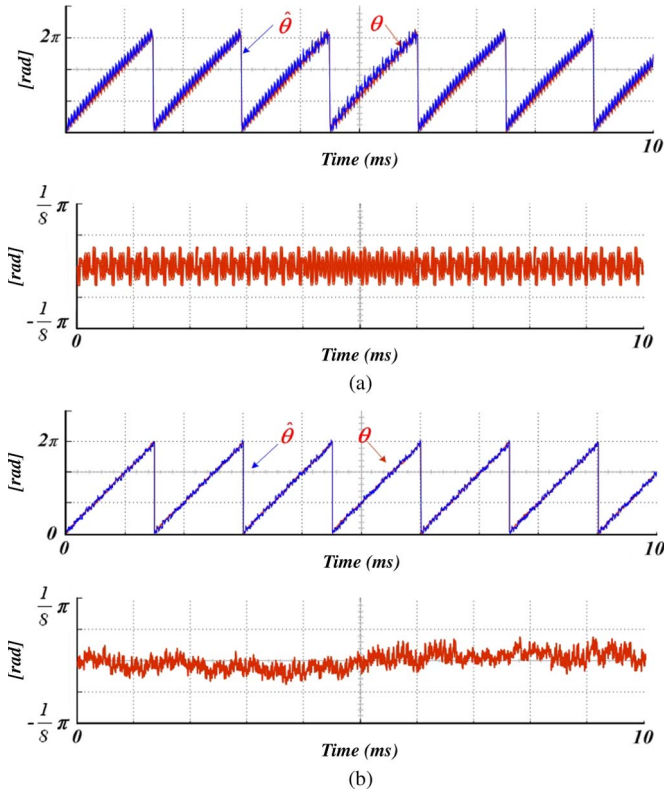


Fig. 12. Experimental data with the inertia load $J_L = 22.3\ \mathrm{kg \cdot cm^2}$. (a) $\hat{\theta}$ and error with signum function. (b) $\hat{\theta}$ and error with sigmoid function.

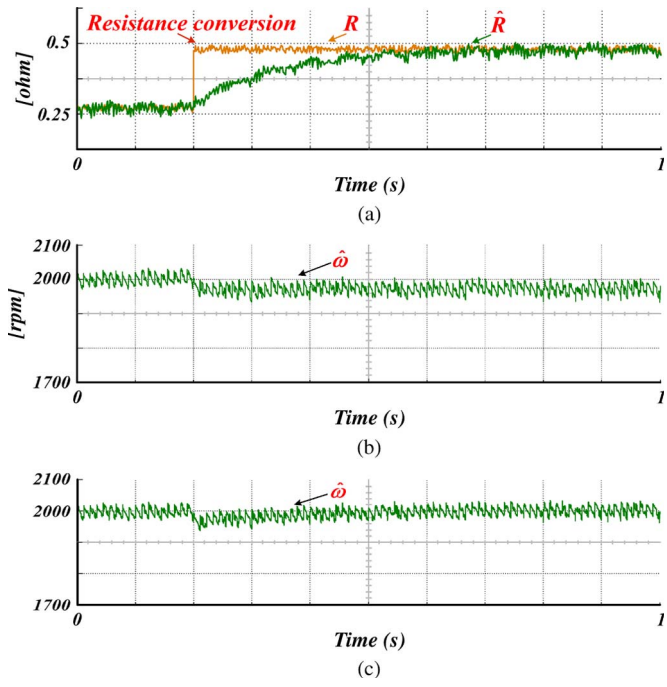


Fig. 13. Velocity tracking with the stator-resistance change. (a) Estimation of the changed resistance. (b) Velocity tracking without the resistance estimation. (c) Velocity tracking with the resistance estimation.

## V. Conclusion

This paper has proposed a new sliding-mode control for a robust sensorless system for a PMSM. The stability of the new SMO has been proved with the use of a Lyapunov stability analysis. The chattering problem in the conventional sliding-mode control was resolved by using a sigmoid function with a variable boundary layer as the switching function instead of the conventional signum function. A stator-resistance estimator was employed to reduce the estimated error associated with parameter fluctuations. The proposed control system has a fast response achieved by reduction of the integral operations needed for the LPF of the conventional adaptive SMO. The superiority of the algorithm has been confirmed through simulations and experiments. In our future research, we will explore the reduction of both overshoot and speed error by the adjustment of gains based on heuristic methods.

## References

[1] P. Pillay and R. Krishnan, "Application characteristics of permanent magnet synchronous and brushless dc motor for servo drive," *IEEE Trans. Ind. Appl.*, vol. 27, no. 5, pp. 986–996, Sep./Oct. 1991.

[2] F. Parasiliti, R. Petrella, and M. Tursini, "Sensorless speed control of a PM synchronous motor by sliding mode observer," in *Proc. IEEE ISIE*, Jul. 1997, vol. 3, pp. 1106–1111.

[3] R. Wu and G. R. Selmon, "A permanent magnet motor drive without a shaft sensor," *IEEE Trans. Ind. Appl.*, vol. 27, no. 5, pp. 1005–1011, Sep./Oct. 1991.

[4] N. Matsui and M. Shigyo, "Brushless dc motor control without position and speed sensor," *IEEE Trans. Ind. Appl.*, vol. 28, no. 1, pp. 120–127, Jan./Feb. 1992.

[5] J. Hu, D. Zhu, Y. D. Li, and J. Gao, "Application of sliding observer to sensorless permanent magnet synchronous motor drive system," in *Proc. IEEE Power Electron. Spec. Conf. Rec.*, Jun. 1994, vol. 1, pp. 532–536.

[6] C. Li and M. Elbuluk, "A sliding mode observer for sensorless control of permanent magnet synchronous motors," in *Conf. Rec. IEEE IAS Annu. Meeting*, Sep. 2001, vol. 2, pp. 1273–1278.

[7] V. Utkin and J. Shi, *Sliding Mode Control on Electromechanical Systems*, 1st ed. New York: Taylor & Francis, 1999.

[8] Y. S. Han, J. S. Choi, and Y. S. Kim, "Sensorless PMSM drive with a sliding mode control based adaptive speed and stator resistance estimator," *IEEE Trans. Magn.*, vol. 36, no. 5, pp. 3588–3591, Sep. 2000.

[9] P. Vaclavek and P. Blaha, "Lyapunov function-based flux and speed observer for ac induction motor sensorless control and parameters estimation," *IEEE Trans. Ind. Electron.*, vol. 53, no. 1, pp. 138–145, Feb. 2006.

[10] S. Ichikawa, M. Tomita, S. Doki, and S. Okuma, "Sensorless control of permanent-magnet synchronous motors using online parameter identification based on system identification theory," *IEEE Trans. Ind. Electron.*, vol. 53, no. 2, pp. 363–372, Apr. 2006.

[11] B. Nahid-Mobarakeh, F. Meibody-Tabar, and F.-M. Sargos, "Mechanical sensorless control of PMSM with online estimation of stator resistance," *IEEE Trans. Ind. Appl.*, vol. 40, no. 2, pp. 457–471, Mar. 2004.

[12] S. Chi, Z. Zhang, and L. Xu, "Sliding-mode sensorless control of direct-drive PM synchronous motors for washing machine applications," *IEEE Trans. Ind. Appl.*, vol. 45, no. 2, pp. 582–590, Mar. 2009.

[13] E. Simon, "Implementation of a speed field oriented control of 3-phase PMSM motor using TMS320F240," Texas Instruments, Dallas, TX, Appl. Rep. SPRA588, Sep. 1999.

[14] K. Paponpen and M. Konghirun, "An improved sliding mode observer for speed sensorless vector control drive of PMSM," in *Proc. CES/IEEE 5th Int. Power Electron. Motion Control Conf.*, Aug. 2006, vol. 2, pp. 1–5.

[15] M. Ertugrul, O. Kaynak, A. Sabanovic, and K. Ohnishi, "A generalized approach for Lyapunov design of sliding mode controller for motion applications," in *Proc. AMC-MIE Conf.*, Mar. 1996, vol. 1, pp. 407–412.

[16] A. Pisano, A. Davila, L. Fridman, and E. Usai, "Cascade control of PM DC drives via second-order sliding-mode technique," *IEEE Trans. Ind. Electron.*, vol. 55, no. 11, pp. 3846–3854, Nov. 2008.

[17] K. C. Veluvolu and Y. C. Soh, "High-gain observers with sliding mode for state and unknown input estimations," *IEEE Trans. Ind. Electron.*, vol. 56, no. 9, pp. 3386–3393, Sep. 2009.

[18] Y. Feng, J. Zheng, X. Yu, and N. Truong, "Hybrid terminal sliding-mode observer design method for a permanent-magnet synchronous motor control system," *IEEE Trans. Ind. Electron.*, vol. 56, no. 9, pp. 3424–3431, Sep. 2009.

[19] B. K. Kim, W. K. Chung, and K. Ohba, "Design and performance tuning of sliding-mode controller for high-speed and high-accuracy positioning systems in disturbance observer framework," *IEEE Trans. Ind. Electron.*, vol. 56, no. 10, pp. 3798–3809, Oct. 2009.
[20] X. Yu and O. Kaynak, "Sliding-mode control with soft computing: A survey," *IEEE Trans. Ind. Electron.*, vol. 56, no. 9, pp. 3275–3283, Sep. 2009.
[21] C. Lascu and G.-D. Andreescu, "Sliding-mode observer and improved integrator with dc-offset compensation for flux estimation in sensorless-controlled induction motors," *IEEE Trans. Ind. Electron.*, vol. 53, no. 3, pp. 785–794, Jun. 2006.
[22] M. S. Zaky, M. M. Khater, S. S. Shokralla, and H. A. Yasin, "Wide-speed-range estimation with online parameter identification schemes of sensorless induction motor drives," *IEEE Trans. Ind. Electron.*, vol. 56, no. 5, pp. 1699–1707, May 2009.
[23] Y. S. Kim, S. L. Ryu, and Y. A. Kwon, "An improved sliding mode observer of sensorless permanent magnet synchronous motor," in *Proc. SICE Annu. Conf.*, Aug. 2004, pp. 192–197.
[24] G. Foo and M. F. Rahman, "Sensorless sliding-mode MTPA control of an IPM synchronous motor drive using a sliding-mode observer and HF signal injection," *IEEE Trans. Ind. Electron.*, vol. 57, no. 4, pp. 1270–1278, Apr. 2010.
[25] F. Genduso, R. Miceli, C. Rando, and G. R. Galluzzo, "Back EMF sensorless-control algorithm for high-dynamic performance PMSM," *IEEE Trans. Ind. Electron.*, vol. 57, no. 6, pp. 2092–2100, Jun. 2010.

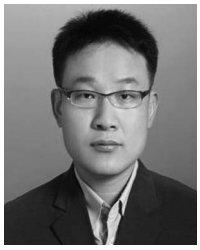

**Hongryel Kim** received the B.S. and M.S. degrees in electronic engineering from Dong-Eui University, Busan, Korea, in 1998 and 2000, respectively. Currently, he is working toward the Ph.D. degree in electronic engineering at Pusan National University, Busan.

His current research interests microprocessor application and system design, distributed control, motion, and motor drive control.

**Jubum Son** received the B.S. degree in mechatronics engineering from Dongmyung University, Busan, Korea, in 2008 and the M.S. degree in mechatronics cooperative from Pusan National University, Busan, in 2010.

He is currently with LS Industrial System, Anyang, Korea. His current research interests include motor drive control, intelligent control system, and microprocessor application control.

**Jangmyung Lee** (M'85–SM'03) received the B.S. and M.S. degrees in electronic engineering from Seoul National University, Seoul, Korea, in 1980 and 1982, respectively, and the Ph.D. degree in computer engineering from the University of Southern California, Los Angeles, in 1990.

Since 1992, he has been a Professor with the Intelligent Robot Laboratory, Pusan National University, Busan, Korea, where he is also the Head of the School of Electrical Engineering. His current research interests include intelligent robotic systems, transport robot, and intelligent sensors and control algorithms.

Dr. Lee was the former Chairman of the Research Institute of Computer Information and Communication. He is currently the President of the Korea Robotics Society.